


Breakthrough of regenerative chatter modeling in milling by including unexpected effects arising from tooling system deflection

Giovanni Totis¹ 

Received: 29 July 2016 / Accepted: 1 December 2016 / Published online: 14 December 2016
© Springer-Verlag London 2016

Abstract Self-excited anomalous vibrations called chatter affected milling operations since the beginning of the industrial era. Chatter is responsible for bad surface quality of the machined part and it may severely damage machining system elements. Although the significant advances of recent years, state of the art dynamic models are not yet able to completely explain chatter onset even when some conventional cutting tools are applied for conventional milling operations. In this work, a more general model of regenerative chatter is presented. The model takes into account some additional degrees of freedom and cutting forces which are neglected in the classical approach. By so doing, a more accurate representation of milling dynamics is obtained, especially when considering large diameter cutters. An improved mathematical formulation of regenerative cutting forces is provided with respect to a very recent publication where the new model has been first outlined. This approach allows -45% of computation time. Moreover, here a new, independent, and stronger experimental validation is provided, where the new model successfully predicts an increase of about $+(50 \div 100)\%$ of the stability boundaries with respect to the classical prediction, thus showing the potential breakthrough of the new approach.

Keywords Milling · Dynamics · Modeling · Chatter · Regenerative effect · Prediction

1 Introduction

Self-excited chatter vibrations in machining were already recognized by F.W. Taylor at the beginning of the nineteenth century as one of “most obscure and delicate of all problems facing the machinist.”

Chatter is caused by complicated physical mechanisms and it is responsible for an unacceptable surface quality and poor dimensional accuracy of the machined parts [1, 2]. Besides, it may accelerate tool wear rate, it may trigger a sudden tool breakage or damage other machine tool components. For these reasons, chatter occurrence must be avoided.

In the last 60 years, several strategies have been developed for solving this awkward problem: passive approaches [3–5], semi-active strategies [6–8], active techniques [9, 10], hybrid strategies based on chatter onset detection and cutting parameters regulation (<http://www.okuma.com/machining-navi>) [11], and predictive strategies based on a preventive evaluation of process stability for an optimal selection of adequate cutting parameters [12–14].

The effectiveness of these techniques relies on the theoretical understanding and accurate modeling of the physical phenomena implying chatter vibrations. Chatter mechanisms are usually classified as primary or secondary.

In the low spindle speed range, chatter onset is mostly influenced by the so called primary chatter mechanisms [21, 22], such as process damping [16, 17], chaotic dynamics of the cutting process [18, 19], effective stress distribution on the normal rake face [1], thermoplastic behavior of the chip material [20], and others.

Especially in the medium-high spindle speed regime, secondary chatter is dominant, which is caused by the regenerative effect. The regenerative effect is the influence of the undulation left on the workpiece by the previous tooth

✉ Giovanni Totis
giovanni.totis@uniud.it

¹ Polytechnical Department of Engineering and Architecture,
University of Udine, Via delle Scienze, 206,
33100 Udine, Italy

passage on the actual uncut chip thickness acting on the tooth passing through the same angular position [1, 2, 15].

According to all current models, the instantaneous chip thickness evaluation on a given cutting tooth is performed by only considering tool tip transversal vibrations in the working plane orthogonal to spindle axis.

One very recent exception is the work of Kilic et al. [34] presenting a generalized model for cutting mechanics and dynamics which theoretically includes all possible translational and rotational degrees of freedom (six in total) for accurately modeling regenerative chip thickness in generic conditions. However, the consequence of this idea in conventional face milling with large diameter cutters was not investigated.

In addition, only the transverse forces are taken into account for modeling tooling system deflection, while the momenta associated to the axial forces are always neglected.

Considering only transverse vibrations and transverse forces is a reasonable approximation when considering slender tooling systems with a small cutter diameter D in comparison to the total tool overhang L .

Nevertheless, when considering tooling systems with a relatively large D/L ratio, this simplification may be too rough and it may cause great inaccuracies when computing the stability boundaries by means of predictive algorithms.

In a very recent work [24], an innovative model of milling dynamics was proposed for overcoming the limits of the classical approach by taking into account additional degrees of freedom for a better description of tooling system bending as well as the bending momenta deriving from axial forces.

In [24], the model was successfully validated by performing several experimental tests on a face milling cutter with $D = 80$ mm, total overhang $L = 300$, $Z_t = 4$ teeth, and working cutting edge angle $\chi_1 = 90^\circ$. Process stability was evaluated with different nose radii ($r_\varepsilon = 0.4$ mm and $r_\varepsilon = 2$ mm). When adopting the larger nose radius, a significant shift of the stability borders of about +25 % was experimentally observed and correctly predicted by the new approach. Further details can be found in [24].

Thus, the proposed model significantly improved the accuracy of the predicted stability borders when considering tools with a relatively large D/L ratio and with curved or inclined cutting edges (average local $\chi < 90^\circ$).

In this work, a new mathematical formulation of the model introduced in [24] will be provided, which will almost halve the computation time. Specifically, an integral formulation of the regenerative cutting force coefficients will be presented together with analytical direct formulas for standard cutting inserts defined by the nominal working cutting edge angle χ_1 and by the nose radius r_ε . In addition, a new, independent, and stronger experimental validation of the new model will be presented in this work.

First of all, a review on regenerative chatter modeling in milling will be outlined. Subsequently, the extended model of milling dynamics proposed in [24] will be recalled. Afterwards, a novel, improved mathematical formulation describing cutter-workpiece dynamic interaction will be presented. The criteria for stability evaluation will be synthetically described. Eventually, another impressive experimental validation of the new model will be discussed in the last sections.

2 State of the art approaches for modeling and simulation of regenerative chatter in milling

The global transfer function of the machining system is mainly dependent on the most flexible element of the kinematic chain, which is typically the tooling system [25]. However, when milling turbine blades or other thin parts, workpiece dynamics have to be taken into account, as proved in [26, 27].

The most simple dynamic milling model is based on a single oscillating direction described by a single harmonic oscillator [28, 29]. Nevertheless, the validity of this model is limited to very few industrial cases. A typical milling process is at least bidimensional, having at least one harmonic oscillator for each direction, as was shown in the pioneering work of Altintas and Budak [23] and in many other research works [12, 30].

However, in many practical cases, several harmonic oscillators are necessary for each direction, in order to model machining system dynamics with sufficient accuracy [14, 16, 31–33].

Cutting forces tend to amplify regenerative vibrations, thus a correct modeling of cutting forces is crucial. In particular, cutting force variations due to regenerative perturbations have to be accurately described. Several approaches have been proposed in literature in the last decades, see for instance [34]. In this work, a compact Shearing & Ploughing linear model based on some basic oblique cutting hypotheses will be adopted [34–37].

Process kinematics have a great impact on milling dynamics. For instance, the stability borders are influenced by milling configuration (up or down milling [29]), by the radial immersion between tool and workpiece a_L/D [30] and by other kinematic parameters.

Last but not least, the regenerative effect is influenced by the geometrical details of the cutter, as illustrated in [32, 38–40], which affect the dynamic interaction between tool and workpiece.

According to the classical approach, regenerative chatter does only depend on the transverse vibrations and forces between tool and workpiece in the working plane orthogonal to spindle axis. This assumption is valid for the slender

tooling systems with a small D/L ratio extensively studied in literature [12, 30, 38, 40].

As outlined in the introduction, the widespread approach of considering only transverse vibrations and forces was recently overcome by Kilic et al. [34], who pointed out the necessity of taking into account all possible degrees of freedom which may influence the local, instantaneous chip thickness. The authors successfully explored this illuminating idea in some conventional and less conventional machining operations. Nevertheless, the consequence of their generalized approach in conventional face milling with large diameter cutters was neither investigated, nor implemented or validated.

Inspired by this idea, the model presented of [24] was then conceived and validated, including additional degrees of freedom for a realistic chip thickness evaluation and bending momenta due to axial forces.

Eventually, it is worth recalling that the theoretical stability boundaries are obtained by performing the stability analysis on the global dynamic milling model including the regenerative effect. Stability analysis can be carried out by performing time domain simulations or other linear numerical methods. Time domain simulations are more realistic since they can model non-linear phenomena such as the loss of contact between tooth and workpiece, the multiple regenerative effect, the nonlinear cutting force trend versus uncut chip thickness [41, 42]. Nevertheless, they are very time consuming and thus they are not adequate for

most industrial applications. Accordingly, the most common approach is to perform a linear analysis of stability by means of efficient DDE-based techniques [8], as done in this work.

3 New model of milling dynamics

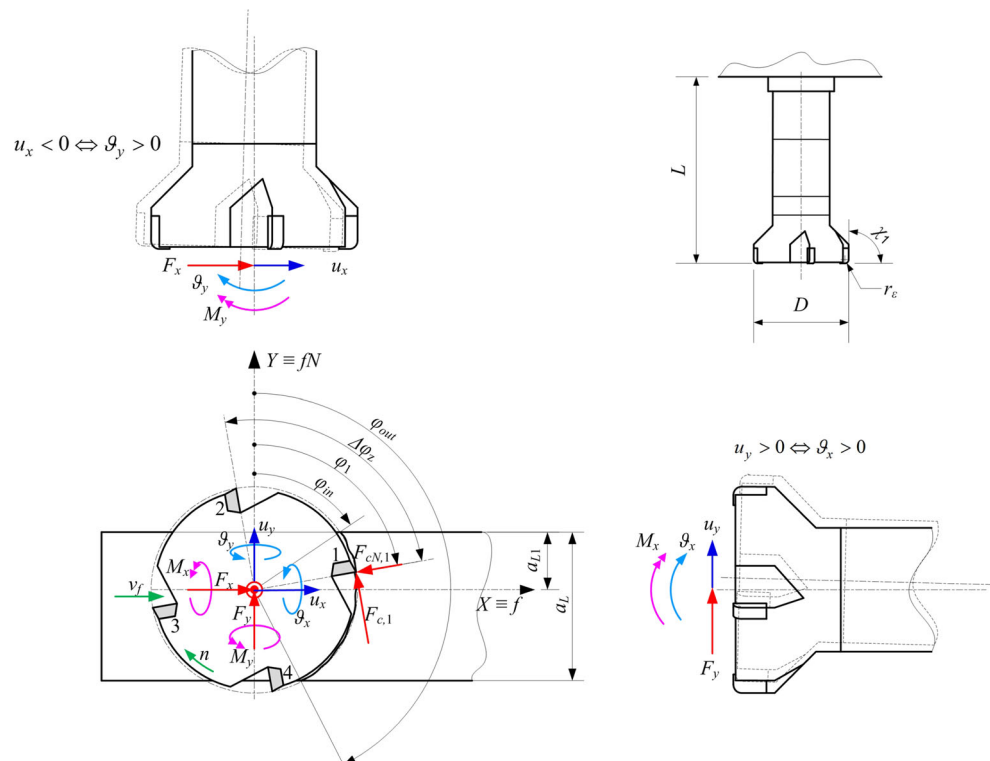
In this section, a new dynamic milling model will be introduced.

Classically

$$\begin{aligned} \begin{bmatrix} u_x \\ u_y \end{bmatrix} &= \begin{bmatrix} W_{uxFx} & W_{uxFy} \\ W_{uyFx} & W_{uyFy} \end{bmatrix} \begin{bmatrix} F_x \\ F_y \end{bmatrix} \\ &\approx \begin{bmatrix} W_{uxFx} & 0 \\ 0 & W_{uyFy} \end{bmatrix} \begin{bmatrix} F_x \\ F_y \end{bmatrix} \end{aligned} \tag{1}$$

Let us consider a generic spindle-toolholder-cutter system for milling operations, as illustrated in Fig. 1. Due to mechanical vibrations, the cutter tip barycentre translates in the working XY plane perpendicular to spindle axis, but at the same time cutter body may also rotate in the Cartesian planes XZ and YZ . These rotations are usually neglected in the technical literature; on the contrary, this research work will prove their fundamental role for milling dynamics modeling and chatter forecast, especially when considering large diameter cutters. The system is considered rigid in the axial and torsional directions. For the sake of simplicity, the workpiece is also considered to be rigid.

Fig. 1 Reference scheme for relative tool-workpiece vibrations



In the Fourier domain, the following dynamic relation can be obtained

$$\begin{bmatrix} u_x \\ \vartheta_y \\ u_y \\ \vartheta_x \end{bmatrix} = \begin{bmatrix} W_{uxFx} & W_{uxMy} & W_{uxFy} & W_{uxMx} \\ W_{\vartheta_yFx} & W_{\vartheta_yMy} & W_{\vartheta_yFy} & W_{\vartheta_yMx} \\ W_{uyFx} & W_{uyMy} & W_{uyFy} & W_{uyMx} \\ W_{\vartheta_xFx} & W_{\vartheta_xMy} & W_{\vartheta_xFy} & W_{\vartheta_xMx} \end{bmatrix} \begin{bmatrix} F_x \\ M_y \\ F_y \\ M_x \end{bmatrix} \tag{2}$$

where all the quantities are functions of the imaginary axis $j\omega$. The bending moments M_x and M_y will arise from the axial forces acting on cutter teeth, which may be significant when nose radius r_ϵ is high or when the working angle χ is relatively small, as will be described in the next sections.

Each transfer function can be expressed as a sum of harmonic oscillators, i.e.,

$$W(j\omega) = \sum_{k=1}^M \frac{G_k}{(j\omega / \omega_{n,k})^2 + 2\xi_k(j\omega / \omega_{n,k}) + 1} \tag{3}$$

where G_k is the zero frequency gain or static compliance, $\omega_{n,k}$ is the natural pulsation, and ξ_k is the damping coefficient of the k_{th} mode of vibration. In general, the modal parameters may change from one transfer function to the other. However, some assumptions will be adopted for model optimization, as will be explained in the following.

3.1 Basic reference model based on Euler-Bernoulli beam element

Let us consider a finite element beam with circular cross section based on Euler-Bernoulli model, in cantilever configuration, whose length L and external diameter d correspond to the total tooling system overhang (from spindle nose to cutter tip) and average diameter, as illustrated in Fig. 2. Let E be the Young modulus and J be the moment of inertia given by

$$J = \frac{\pi d^4}{64} \tag{4}$$

Let u and ϑ be the radial displacement and rotation of beam free tip, where the radial force F and the moment M can be applied. From the Euler-Bernoulli theory, one can easily derive the following static compliance relations

$$\begin{cases} u = \frac{L^3}{3EJ} F + \frac{L^2}{2EJ} M = H_{uF} F + H_{uM} M \\ \vartheta = \frac{L^2}{2EJ} F + \frac{L}{EJ} M = H_{\vartheta F} F + H_{\vartheta M} M \end{cases} \tag{5}$$

It is worth noting that all static compliance can be expressed as proportional to the displacement-force flexibility, as follows

$$\begin{cases} H_{uM} = \nu H_{uF} \\ H_{\vartheta F} = \nu H_{uF} \\ H_{\vartheta M} = \mu H_{uF} \end{cases} \tag{6}$$

where

$$\nu = \frac{3}{2L}; \quad \mu = \frac{3}{L^2} \tag{7}$$

If we consider the dynamic Euler-Bernoulli beam element including inertial and damping matrixes, we will finally obtain the dynamic version of Eq. 5. Specifically, one obtains

$$\begin{cases} u(j\omega) = W_{uF}(j\omega) F(j\omega) + W_{uM}(j\omega) M(j\omega) \\ \vartheta(j\omega) = W_{\vartheta F}(j\omega) F(j\omega) + W_{\vartheta M}(j\omega) M(j\omega) \end{cases} \tag{8}$$

It can be easily shown that each transfer function of this model encloses two resonances. Since the first, low-frequency resonance is dominant in our case, it will be sufficient to focus on that in order to get a realistic representation of system dynamics. Under this assumption, the following simplification can be carried out

$$\begin{cases} W_{uM}(j\omega) \approx \nu W_{uF}(j\omega) \\ W_{\vartheta F}(j\omega) \approx \nu W_{uF}(j\omega) \\ W_{\vartheta M}(j\omega) \approx \mu W_{uF}(j\omega) \end{cases} \tag{9}$$

In other words, the dynamic transfer functions are approximately proportional to the displacement-force transfer function, by means of the same constants.

In most cases, the effect of M on ϑ through $W_{\vartheta M}$ is negligible, since μ or M are small. As a consequence, the following important relation holds

$$\vartheta(j\omega) \approx \nu u(j\omega) \tag{10}$$

Another important topic is the determination of the radial displacement u_r as well as the axial displacement u_a of the cutter tooth located at $D/2$ from tooling system axis. According to signs conventions adopted in Fig. 2, they are given by

$$\begin{cases} u_r(j\omega) = u(j\omega) \\ u_a(j\omega) = -\frac{D}{2} \vartheta(j\omega) \end{cases} \tag{11}$$

Moreover, let us suppose that the equivalent nodal forces depend on the radial F_r and axial F_a forces shown in Fig. 2, which are applied at $D/2$ from beam axis. Thus,

$$\begin{cases} F(j\omega) = F_r(j\omega) \\ M(j\omega) = -\frac{D}{2} F_a(j\omega) \end{cases} \tag{12}$$

where it should be recalled that in general $D \neq d$, since D is the external cutter diameter while d is the tooling system average diameter.

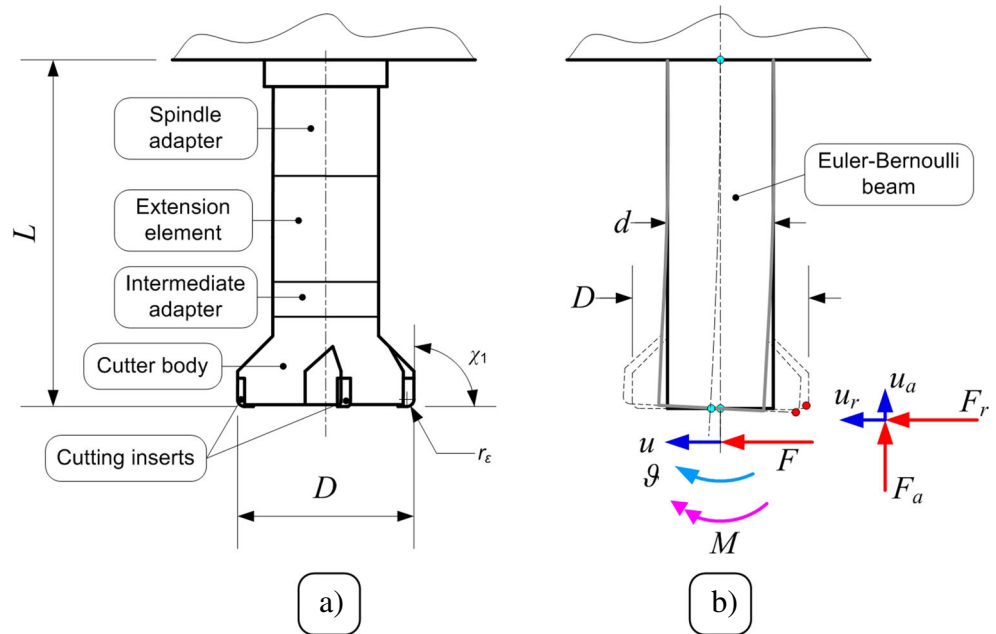
Therefore, after some algebraic manipulations, one may obtain

$$\begin{cases} u_r(j\omega) \approx W_{uF}(j\omega) [F_r(j\omega) - \eta F_a(j\omega)] \\ u_a(j\omega) \approx W_{uF}(j\omega) [-\eta F_r(j\omega) + \lambda F_a(j\omega)] \end{cases} \tag{13}$$

where

$$\eta = \frac{3D}{4L}, \quad \lambda = \frac{3}{4} \left(\frac{D}{L}\right)^2 \tag{14}$$

Fig. 2 **a** Example of a typical tooling system. **b** Basic model based on a single Euler-Bernoulli beam



are aspect ratio factors which will be very important in the following. If we assume a realistic aspect ratio of about

$$\frac{D}{L} \approx \frac{1}{3} \Rightarrow \eta \approx 25\%, \quad \lambda \approx 8\% \tag{15}$$

Under this hypothesis, the influence of the axial force on the transverse displacement cannot be ignored. Specifically, it tends to reduce the destabilizing effect of the radial force. Thus, the axial force may play a fundamental role for increasing cutting process stability. This is an empirical fact which is relatively known among technicians working in the shop-floor. Nevertheless, this fact has not been adequately explained and demonstrated in literature until the very recent work of Totis et al. [24].

Under the above hypothesis, it should also be noticed that the size of the axial displacement cannot be neglected in comparison with the radial displacement. Eventually, the effect of axial force on axial displacement is practically negligible since λ is small (see Eq. 14).

3.2 Tooling system dynamics during rotation

Let us now model the effective dynamics of the cutter during rotation. According to the classical approach, only the transverse vibrations u_x and u_y of cutter barycentre are necessary to model cutting process dynamics. The new model extends this approach to the 3D case, where also the axial vibrations $u_{z,j}$ of each tooth may influence the onset of chatter phenomena. The proposed model reduces to the conventional one when the D/L ratio is small, as in the case of slender endmills for finishing applications. Nevertheless, when using large diameter cutters, such as those

adopted for roughing applications, the $u_{z,j}$ vibrations will become significant, thus affecting the evolution of vibrational phenomena, as it will be proved in the last sections.

$$\begin{cases} u_{x,j}(j\omega) = H_{uxFx}(j\omega) F_x(j\omega) - H_{uxMy}(j\omega) M_y(j\omega) \\ u_{y,j}(j\omega) = H_{uyFy}(j\omega) F_y(j\omega) + H_{uyMx}(j\omega) M_x(j\omega) \end{cases} \tag{16}$$

where the displacement-moment transfer functions are assumed proportional to the direct transfer functions H_{uxFx} and H_{uyFy} , respectively, as follows

$$\begin{cases} H_{uxMy}(j\omega) \approx \nu_y H_{uxFx}(j\omega) \\ H_{uyMx}(j\omega) \approx \nu_x H_{uyFy}(j\omega) \end{cases} \tag{17}$$

In accordance with the Euler-Bernoulli toy model of previous subsection (10), the cutter body small rotations ϑ_x and ϑ_y in the ZY and ZX cartesian planes are assumed proportional to the transverse vibrations u_x and u_y —by means of the same proportionality constants ν_y and ν_x —as follows

$$\begin{cases} \vartheta_y(j\omega) \approx -\nu_y u_x(j\omega) \\ \vartheta_x(j\omega) \approx \nu_x u_y(j\omega) \end{cases} \tag{18}$$

where

$$\nu_y \cong \nu_x \cong \frac{3}{2L} \tag{19}$$

Finally, the axial vibrations of the j th tooth can be computed in the time domain using the following relation

$$u_{z,j}(t) = R \cos(\varphi_j(t)) \vartheta_x(t) - R \sin(\varphi_j(t)) \vartheta_y(t) \tag{20}$$

where φ_j is the feed motion angle of the j th tooth and R is the local radius where the considered cutting edge

point is located. For face milling cutters with cemented carbide inserts, this radius is approximately constant along the whole cutting edge, and it is $R \cong \frac{D}{2}$, where D is the external cutter diameter.

4 Cutting force model

Cutting forces depend on several factors, such as workpiece material, cutting parameters, cutter geometry, and milling process geometry. Let us consider a milling operation performed with a constant pitch milling cutter with Z_t cutting inserts or flutes, nominal working cutting edge angle χ_1 , nose radius r_ϵ , and axial rake angle γ_a .

Let us further assume that the variation of the angular localization of a given cutting edge due to axial rake is negligible, which is true if

$$a_p \gamma_a \ll \pi D \tag{21}$$

in the case of inserted cutters for face milling.

Let us suppose constant speed machining conditions, i.e., no modulation of spindle speed is applied.

Under these assumptions, the local cutting edge geometry cannot be considered constant along the engaged cutting edge.

Let us now model the cutting forces acting on the infinitesimal cutting edge length dl at point P on the j th flute at a given time instant t .

For this purpose, let us firstly introduce the angular spindle speed Ω expressed in rad/s. Under constant spindle speed conditions,

$$\Omega = \frac{2\pi n}{60} = \frac{2\pi}{T} \tag{22}$$

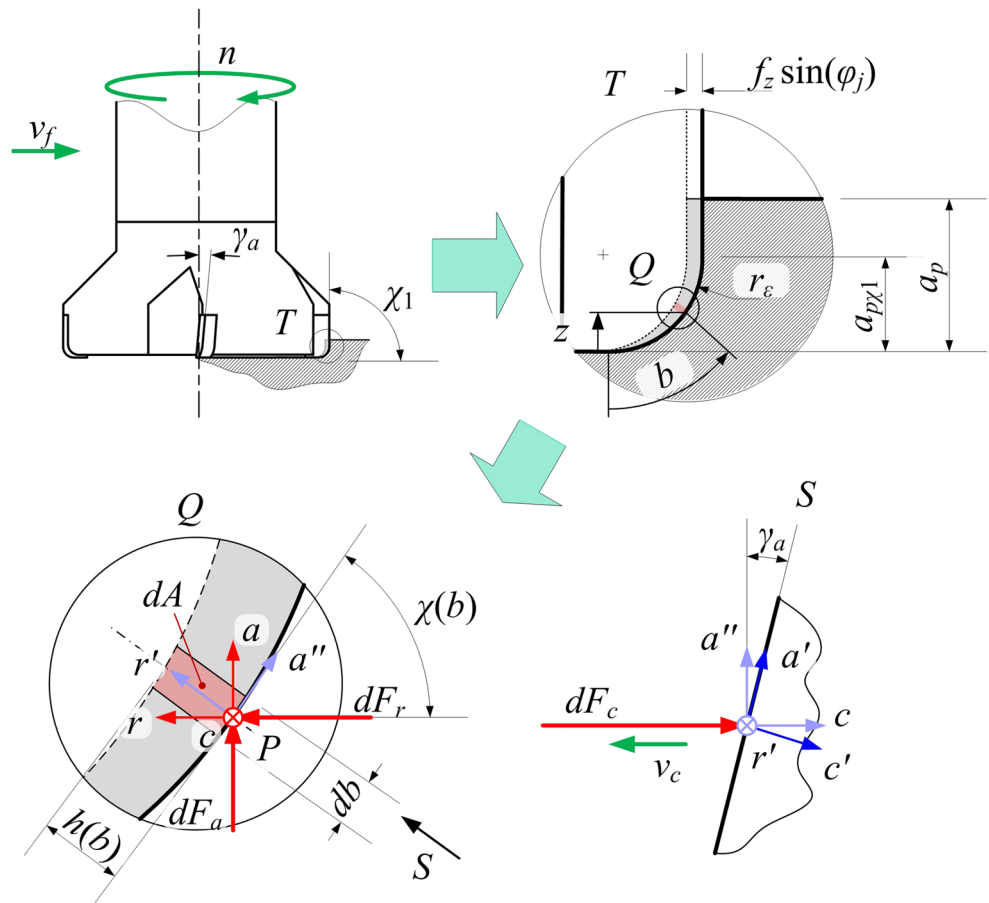
n being the (constant) spindle speed expressed in rpm and T the (constant) spindle revolution period. Let us introduce the time delay between subsequent teeth τ . Under the hypothesis of constant speed machining and an equally spaced teeth cutter, the time delay τ is given by

$$\tau = \frac{T}{Z_t} = \frac{60}{n Z_t} \tag{23}$$

where Z_t is the teeth number.

Let us consider a generic cutting edge point P on tooth j , as shown in Fig. 3. In cylindrical coordinates P is univocally

Fig. 3 Local reference frames for cutter geometry characterization and cutting force modeling



determined by its height z_P along tool axis, its local radius $R(z_P)$ and its local feed motion angle

$$\varphi_j(t, z_P) \approx \varphi_j(t, z = 0) = \varphi_j(t) \quad \forall z \quad (24)$$

where the dependence of the feed motion angle on the z coordinate can be suppressed thank to assumption (21).

Under the hypothesis of equally spaced teeth, we have

$$\varphi_j(t) = \varphi_1(t) - (j - 1) \Delta\varphi_z, \quad j = 1, 2, \dots, Z_t \quad (25)$$

where $\Delta\varphi_z$ is the angular pitch (angular delay) between subsequent teeth, which is given by

$$\Delta\varphi_z = \frac{2\pi}{Z_t} \quad (26)$$

In order to identify the angular position of the cutter, it is possible to consider the feed motion angle of the first flute tip as main reference, which will be simply denoted by φ in the following, i.e.,

$$\varphi(t) = \varphi_1(t) \quad (27)$$

The engagement of each tooth part in the workpiece will be described through the window function g_j , as follows

$$g_j(t) = g(\varphi_j(t)) = \begin{cases} 1 & \text{if } \varphi_{in} < \varphi_j < \varphi_{out} \\ 0 & \text{elsewhere} \end{cases} \quad (28)$$

being φ_{in} and φ_{out} the entrance and exit angles, respectively, recalling that $\varphi_j \in [0, 2\pi]$.

Let us further define

$$\begin{cases} s_j = \sin(\varphi_j(t)) \\ c_j = \cos(\varphi_j(t)) \end{cases} \quad (29)$$

Let us now consider the working plane π_f passing through P , which is perpendicular to tool axis and parallel to the stationary plane OXY . This plane does also contain the direction of the local cutting speed v_c . It is possible to define a local reference frame cra , where the unit vector c is parallel to the tangential cutting speed v_c , r is the radial unit vector, and a is the axial unit vector parallel to tool axis.

Under generic conditions, the cutting edge may be inclined. Its orientation is univocally determined by the local working cutting edge angle χ and by the local axial rake angle γ_a (also called helix angle and sometimes denoted by λ or ι).

The rotation of the reference system cra of an angle equal to χ around the c direction yields a new radial unit vector r' . After another rotation of the new reference frame of an angle equal to γ_a around r' , the final $c'r'a'$ reference frame is obtained, which will be important for the oblique cutting force model described in the following.

It is worth noting that the local cutting edge angle may in general vary along the cutting edge – even for face shoulder

cutters with nominal cutting edge angle $\chi = 90^\circ$ – because of the nose radius r_ϵ . In this work, this case is deeply investigated. Besides, the axial rake angle γ_a may in general vary along the cutting edge.

Under an infinitesimal variation dz along the j th flute, the true cutting edge length is given by

$$dl = \frac{dz}{\sin \chi \cos \gamma_a} \quad (30)$$

Another important quantity is the projection of dl on the ra plane, that is

$$db = dl \cos \gamma_a = \frac{dz}{\sin \chi} \quad (31)$$

For the sake of cutting force modeling, it is better to take b as the main curvilinear abscissa, i.e.,

$$z \rightarrow b(z) \quad (32)$$

Accordingly, let us consider an infinitesimal (projected) cutting edge length db located at b , where the instantaneous chip thickness is

$$h_j = h_j(t, b) \quad (33)$$

while the infinitesimal chip cross-section area is given by

$$dA_j(b) = h_j(t, b) db \quad (34)$$

As stated above, in general

$$\chi = \chi(b) \quad \text{and} \quad \gamma_a = \gamma_a(b) \quad (35)$$

However, the b dependence as well as the time dependence of other variables may be omitted in the following, in order to simplify notation.

A linear cutting force model is adopted, which is inspired by some modern Shearing & Ploughing cutting force models which are also based on oblique cutting principles [34–37]. Infinitesimal cutting forces acting on the cutting edge part db are mainly due to effect of chip pressure on rake face (shearing terms) and the effect of dynamic Coulomb friction between the main clearance and the machined surface (ploughing terms). Specifically, the chip pressure on rake face causes:

- a force approximately perpendicular to rake face (i.e., parallel to the c' direction), represented by $k_{cs}dA_j$;
- a force approximately parallel to rake face, i.e., perpendicular to the cutting edge along the r' direction, represented by $k_{ns}dA_j$.

At the same time, the dynamic Coulomb friction between the main clearance and the machined surface causes the following ploughing terms:

- a force perpendicular to clearance, i.e., practically parallel to the r' direction, which is represented by $k_{np}db$ term;
- a force parallel to the relative motion direction represented by c or v_c , which is given by $k_{cp}db$. As a consequence, this force has a non-zero projection on both c' and a' directions.

Accordingly, the infinitesimal forces acting on db in the $c'r'a'$ reference system are

$$\begin{cases} dF_{c',j} \cong k_{cs}dA_j + k_{cp} \cos \gamma_a db \\ dF_{r',j} \cong k_{ns}dA_j + k_{np}db \\ dF_{a',j} \cong k_{cp} \sin \gamma_a db \end{cases} \quad (36)$$

The above physical considerations based on this simple Coulomb friction model suggest the following prediction

$$\frac{k_{ns}}{k_{cs}} \approx \frac{k_{cp}}{k_{np}} \approx 0.1 \div 1 \quad (37)$$

which was experimentally confirmed by the S&P coefficients estimated in technical literature [14, 51], which are approximately within the following ranges

$$\begin{aligned} k_{cs} &= (0.8 \pm 0.2) k_s; & k_{ns} &= (0.45 \pm 0.3) k_{cs}; \\ k_{np} &= (0.05 \pm 0.04) k_{cs}; & k_{cp} &= (0.6 \pm 0.35) k_{np} \end{aligned} \quad (38)$$

where k_s is the cutting pressure F_c/A ; k_s , k_{cs} , and k_{ns} are expressed in (N/mm²), while k_{cp} and k_{np} are expressed in (N/mm).

It has to be noticed that the dynamic ploughing terms responsible for process damping [16, 37] were not considered here, since process damping was neglected in this treatment. However, process damping terms can be easily included in future extensions of this model.

After reference system rotation of γ_a around r' and of χ around c direction, the force components in the cra reference system are obtained, as follows

$$\begin{cases} dF_{c,j} \cong k_{cs}dA_j \cos \gamma_a + k_{cp}db \\ dF_{r,j} \cong k_{ns}dA_j \sin \chi + k_{np}db \sin \chi + k_{cs}dA_j \sin \gamma_a \cos \chi \\ dF_{a,j} \cong k_{ns}dA_j \cos \chi + k_{np}db \cos \chi - k_{cs}dA_j \sin \gamma_a \sin \chi \end{cases} \quad (39)$$

It is worth noting that the proposed model incorporates oblique cutting conditions which may occur when the axial rake $\gamma_a \neq 0$. In these circumstances, the new term $k_{cs}dA_j \sin \gamma_a$ arises, which may affect the total cutting force components.

$$\begin{cases} F_{c,j} = \int_0^{B(a_p)} dF_{c,j}(b) \\ F_{r,j} = \int_0^{B(a_p)} dF_{r,j}(b) \\ F_{a,j} = \int_0^{B(a_p)} dF_{a,j}(b) \end{cases} \quad (40)$$

After integration along each cutting edge and addition of all the contributions from each tooth, the resultant cutting force components and momenta are eventually obtained

$$\begin{cases} F_{x,0} = \sum_{j=1}^{Z_t} [-F_{c,j}c_j - F_{r,j}s_j] \\ M_{y,0} = \sum_{j=1}^{Z_t} -F_{a,j}R_sj \\ F_{y,0} = \sum_{j=1}^{Z_t} [F_{c,j}s_j - F_{r,j}c_j] \\ M_{x,0} = \sum_{j=1}^{Z_t} F_{a,j}Rc_j \end{cases} \quad (41)$$

These coefficients constitute the vector of nominal cutting forces F_0 , which is a 4×1 τ or T -periodic vector depending only on the nominal chip thickness.

5 Breakthrough model of cutter-workpiece dynamic interaction

Tool tip vibrations perturb the instantaneous local chip thickness as follows

$$h_j(t, b) = \underbrace{h_{j0}(t, b)}_{\text{nominal, } \tau\text{-periodic}} + \underbrace{h_{j\delta}(t, b)}_{\text{regenerative perturbation}} \quad (42)$$

where the instantaneous nominal chip thickness h_{j0} is given by

$$h_{j0}(t, b) \cong g_j(t, b) f_z s_j(t) \sin \chi(b) \quad (43)$$

being f_z the feed per tooth.

The regenerative perturbation is classically given by

$$h_{j\delta}(t, b) = [u_r(t) - u_r(t - \tau)] \sin \chi(b) \quad (44)$$

where u_r is the transverse vibration projected in the radial direction of the j th tooth.

Nevertheless, when axial vibrations cannot be neglected, new terms arise in the regenerative chip thickness formula, i.e.

$$h_{j\delta}(t, b) = [u_r(t) - u_r(t - \tau)] \sin \chi(b) + [u_a(t) - u_a(t - \tau)] \cos \chi(b) \quad (45)$$

as illustrated in Fig. 4.

In short, this new theoretical result explains the influence of axial vibrations on regenerative chip thickness and thus on process stability.

In the current case, by accepting the coupling between radial and axial vibrations expressed by Eqs. 10 and 11, we finally get

$$h_{j\delta}(t, b) = [\sin \chi(b) - \cos \chi(b) R(b) v] \times [u_r(t) - u_r(t - \tau)] \quad (46)$$

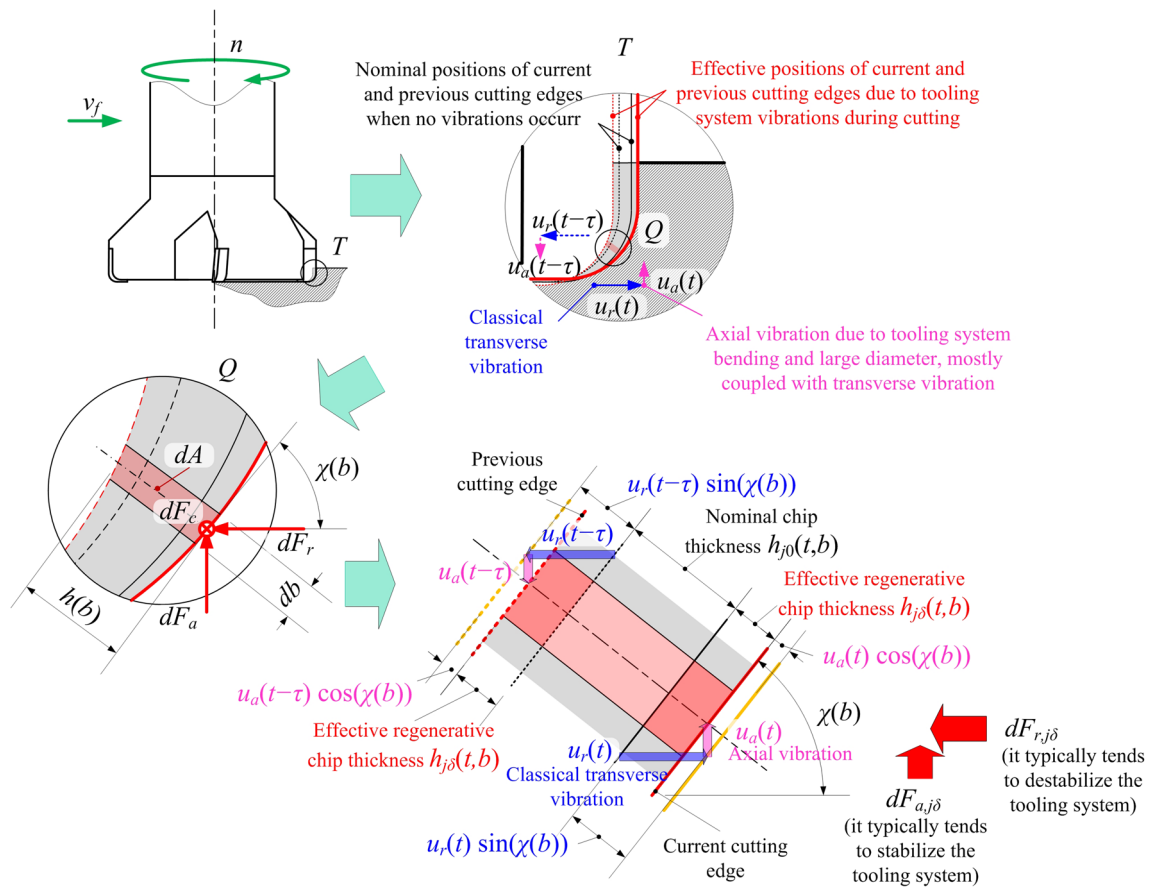


Fig. 4 Schematic representation of regenerative chip thickness behavior on inclined cutting edges, showing the dependence on both radial and axial vibrations

where $R(b)$ is the local radius at the considered abscissa b .

By comparing the new term with the classical term, it yields

$$\frac{\text{new term}}{\text{classical term}} = \frac{\cos \chi R v}{\sin \chi} = \cotg \chi \frac{3D}{4L} \quad (47)$$

For example, in the experimental case study presented in this work—which may represent a typical industrial case—we have

$$\frac{D}{L} \approx \frac{1}{4}, \quad \chi \approx 40^\circ \Rightarrow \frac{\text{new term}}{\text{classical term}} \approx 22\% \quad (48)$$

which is a significative variation with respect to the classical result.

Regenerative cutting forces will depend on the chip thickness perturbations with respect to the “static,” periodic chip thickness h_{j0} . Specifically, cutting forces can be linearized as follows

$$\begin{aligned} dF_{w,j}(t,b) &= dF_{w,j}(h_{j0}(t,b)) \\ &+ \frac{\partial dF_{w,j}}{\partial h_j}(h_{j0}(t,b)) h_{j\delta}(t,b) \\ &= dF_{w,j0}(t,b) + dF_{w,j\delta}(t,b) \quad w = c, r, a \end{aligned} \quad (49)$$

where w is a generic subscript, the first term is due to the nominal chip thickness, while the force perturbation derives from the regenerative effect.

Accordingly, the following relations are obtained

$$\begin{cases} dF_{c,j\delta} = k_{cs} h_{j\delta} \cos \gamma_a db \\ dF_{r,j\delta} = k_{ns} h_{j\delta} \sin \chi db + k_{cs} h_{j\delta} \sin \gamma_a \cos \chi db \\ dF_{a,j\delta} = k_{ns} h_{j\delta} \cos \chi db - k_{cs} h_{j\delta} \sin \gamma_a \sin \chi db \end{cases} \quad (50)$$

Let us now integrate the differential contributions along the cutting edge, by focusing on inserted cutters where it is reasonable to assume that a given cutting edge is well located at φ_j , and under the assumption that the axial rake is almost constant along the cutting edge. Then

$$\begin{cases} F_{c,j\delta}(a_p) = \int_0^{B(a_p)} dF_{c,j\delta} \\ F_{r,j\delta}(a_p) = \int_0^{B(a_p)} dF_{r,j\delta} \\ F_{a,j\delta}(a_p) = \int_0^{B(a_p)} dF_{a,j\delta} \end{cases} \quad (51)$$

which can be expressed as

$$\begin{cases} F_{c,j\delta}(a_p) = k_c(a_p) [u_r(t) - u_r(t - \tau)] \\ F_{r,j\delta}(a_p) = k_r(a_p) [u_r(t) - u_r(t - \tau)] \\ F_{a,j\delta}(a_p) = k_a(a_p) [u_r(t) - u_r(t - \tau)] \end{cases} \quad (52)$$

where

$$k_c(a_p) = \int_0^{B(a_p)} k_{cs} \cos \gamma_a (\sin \chi - Rv \cos \chi) db \quad (53)$$

$$k_r(a_p) = \int_0^{B(a_p)} \left[k_{ns} (\sin^2 \chi - Rv \sin \chi \cos \chi) + k_{cs} \sin \gamma_a (\sin \chi \cos \chi - Rv \cos^2 \chi) \right] db \quad (54)$$

$$k_a(a_p) = \int_0^{B(a_p)} \left[k_{ns} (\sin \chi \cos \chi - Rv \cos^2 \chi) + -k_{cs} \sin \gamma_a (\sin^2 \chi - Rv \sin \chi \cos \chi) \right] db \quad (55)$$

Let us now recall that we are focusing on face milling cutters with mechanically clamped cutting inserts, with nose radius r_ϵ and nominal working cutting edge angle χ_1 . Moreover, axial rake angle is assumed approximately constant along the cutting edge $\gamma_a(b_1) \approx \bar{\gamma}_a$.

Along the nose radius the local working cutting edge varies according to the relation

$$\chi(z = a_p) = \arccos\left(\frac{r_\epsilon - a_p}{r_\epsilon}\right) \quad (56)$$

The endpoint of nose radius—where the straight part of the cutting edge begins, which is oriented according to the nominal working cutting edge angle χ_1 —is located at

$$a_{p\chi 1} = r_\epsilon (1 - \cos \chi_1) \quad (57)$$

In order to analytically determine the regenerative cutting force coefficients of Eqs. 53, 54, and 55, the following integrals are performed, yielding

$$I_{s\chi} = \int_0^{B(a_p)} \sin \chi db = \begin{cases} (-\cos \chi_{ap} + 1) r_\epsilon & \text{if } a_p < a_{p\chi 1} \\ (-\cos \chi_{ap} + 1) r_\epsilon + (a_p - a_{p\chi 1}) & \text{if } a_p \geq a_{p\chi 1} \end{cases} \quad (58)$$

$$I_{c\chi} = \int_0^{B(a_p)} \cos \chi db = \begin{cases} \sin \chi_{ap} r_\epsilon & \text{if } a_p < a_{p\chi 1} \\ \sin \chi_1 r_\epsilon + \cos \chi_1 \left(\frac{a_p - a_{p\chi 1}}{\sin \chi_1}\right) & \text{if } a_p \geq a_{p\chi 1} \end{cases} \quad (59)$$

$$I_{sc\chi} = \int_0^{B(a_p)} \sin \chi \cos \chi db = \begin{cases} \frac{1}{2} \sin^2 \chi_{ap} r_\epsilon & \text{if } a_p < a_{p\chi 1} \\ \frac{1}{2} \sin^2 \chi_1 r_\epsilon + \cos \chi_1 (a_p - a_{p\chi 1}) & \text{if } a_p \geq a_{p\chi 1} \end{cases} \quad (60)$$

$$I_{s2\chi} = \int_0^{B(a_p)} \sin^2 \chi db = \begin{cases} \frac{1}{2} \chi_{ap} r_\epsilon - \frac{1}{4} \sin(2\chi_{ap}) r_\epsilon & \text{if } a_p < a_{p\chi 1} \\ \frac{1}{2} \chi_1 r_\epsilon - \frac{1}{4} \sin(2\chi_1) r_\epsilon + \sin \chi_1 (a_p - a_{p\chi 1}) & \text{if } a_p \geq a_{p\chi 1} \end{cases} \quad (61)$$

$$I_{c2\chi} = \int_0^{B(a_p)} \cos^2 \chi db = \begin{cases} \frac{1}{2} \chi_{ap} r_\epsilon + \frac{1}{4} \sin(2\chi_{ap}) r_\epsilon & \text{if } a_p < a_{p\chi 1} \\ \frac{1}{2} \chi_{ap} r_\epsilon + \frac{1}{4} \sin(2\chi_{ap}) r_\epsilon + \cos^2 \chi_1 \left(\frac{a_p - a_{p\chi 1}}{\sin \chi_1}\right) & \text{if } a_p \geq a_{p\chi 1} \end{cases} \quad (62)$$

Then

$$\begin{cases} k_c(a_p) = k_{cs} \cos \bar{\gamma}_a (I_{s\chi} - I_{c\chi} vR) \\ k_r(a_p) = k_{ns} (I_{s2\chi} - I_{sc\chi} vR) + k_{cs} \sin \bar{\gamma}_a (I_{sc\chi} - I_{c2\chi} vR) \\ k_a(a_p) = k_{ns} (I_{sc\chi} - I_{c2\chi} vR) + -k_{cs} \sin \bar{\gamma}_a (I_{s2\chi} - I_{sc\chi} vR) \end{cases} \quad (63)$$

By recalling that

$$[u_r(t) - u_r(t - \tau)] = [u_x(t) - u_x(t - \tau)] s_j + [u_y(t) - u_y(t - \tau)] c_j \quad (64)$$

one may obtain the regenerative force contributions of the j th tooth in the cra frame

$$F_{c,j\delta} = g_j s_j k_c [u_x(t) - u_x(t - \tau)] + g_j c_j k_c [u_y(t) - u_y(t - \tau)] = F'_{c,jux} [u_x(t) - u_x(t - \tau)] + F'_{c,juy} [u_y(t) - u_y(t - \tau)] \quad (65)$$

and identical relations can be written for $F_{r,j\delta}$ and $F_{a,j\delta}$, by simply substituting k_c with k_r or k_a .

By projecting such terms along the $OXYZ$ stationary reference frame and by summing up the contributions from all the teeth, one obtains the effective regenerative vector \mathbf{F}_δ , i.e.,

$$\mathbf{F}_\delta(t) = \mathbf{F}'_1(t) (\mathbf{u}(t) - \mathbf{u}(t - \tau)) \quad (66)$$

where

$$\mathbf{F}_\delta(t) = \begin{bmatrix} F_{x,\delta}(t) \\ M_{y,\delta}(t) \\ F_{y,\delta}(t) \\ M_{x,\delta}(t) \end{bmatrix}, \quad \mathbf{u}(t) = \begin{bmatrix} u_x(t) \\ u_y(t) \end{bmatrix} \quad (67)$$

$$\mathbf{F}'_1(t) = \begin{bmatrix} F'_{x,jux} & F'_{x,juy} \\ M'_{y,jux} & M'_{y,juy} \\ F'_{y,jux} & F'_{y,juy} \\ M'_{x,jux} & M'_{x,juy} \end{bmatrix} \quad (68)$$

whose time-varying coefficients are given by

$$\left\{ \begin{aligned} F'_{x,jux} &= \sum_{j=1}^{Z_t} (-F'_{c,jux}c_j - F'_{r,jux}s_j) \\ F'_{x,juy} &= \sum_{j=1}^{Z_t} (-F'_{c,juy}c_j - F'_{r,juy}s_j) \\ M'_{y,jux} &= \sum_{j=1}^{Z_t} -F'_{a,jux}Rs_j \\ M'_{y,juy} &= \sum_{j=1}^{Z_t} -F'_{a,juy}Rs_j \\ F'_{y,jux} &= \sum_{j=1}^{Z_t} (F'_{c,jux}s_j - F'_{r,jux}c_j) \\ F'_{y,juy} &= \sum_{j=1}^{Z_t} (F'_{c,juy}s_j - F'_{r,juy}c_j) \\ M'_{x,jux} &= \sum_{j=1}^{Z_t} F'_{a,jux}Rc_j \\ M'_{x,juy} &= \sum_{j=1}^{Z_t} F'_{a,juy}Rc_j \end{aligned} \right. \tag{69}$$

It should be noticed that the matrix F'_1 is τ or T -periodic, depending on whether teeth radial run-out is negligible or not, respectively.

The total force acting on cutter is eventually obtained by summing the static force expressed by Eq. 41 with the regenerative term (67), i.e.,

$$\mathbf{F}(t) = \mathbf{F}_0(t) + \mathbf{F}_\delta(t) \tag{70}$$

Let us consider a state space form (in the time domain) equivalent to Eq. 2, i.e.,

$$\left\{ \begin{aligned} \frac{d\mathbf{q}}{dt}(t) &= \mathbf{A}\mathbf{w}\mathbf{q}(t) + \mathbf{B}\mathbf{w}\mathbf{F}(t) \\ \mathbf{u}(t) &= \mathbf{C}\mathbf{w}\mathbf{q}(t) \end{aligned} \right. \tag{71}$$

where \mathbf{q} is the state vector (with d state variables), $\mathbf{A}\mathbf{w}$, $\mathbf{B}\mathbf{w}$, $\mathbf{C}\mathbf{w}$ are the state space matrices representing a time realization of the transfer function $\mathbf{W}(j\omega)$, \mathbf{F} is the input (force) 4×1 vector, and \mathbf{u} is the output (displacement) 2×1 vector of the tool tip at time t . Time realization is chosen such that tool tip vibrations along X and Y directions can be directly derived from the first two state space variables, that is

$$\left\{ \begin{aligned} u_x &= q_1 \\ u_y &= q_2 \end{aligned} \right. \tag{72}$$

This is achieved when the output matrix of the adopted time realization is

$$\mathbf{C}\mathbf{w} = \begin{bmatrix} 1 & 0 & 0 & \dots & 0 \\ 0 & 1 & 0 & \dots & 0 \end{bmatrix} \tag{73}$$

This choice is particularly important in order to allow monodromy matrix size reduction before eigenvalues computation.

Then the system (71) can be rewritten in the final form

$$\left\{ \begin{aligned} \frac{d\mathbf{q}}{dt} &= \mathbf{A}(t)\mathbf{q}(t) + \mathbf{B}(t)\mathbf{q}(t - \tau) + \mathbf{B}_0(t) \\ \mathbf{u}(t) &= \mathbf{C}\mathbf{q}(t) \end{aligned} \right. \tag{74}$$

where $\mathbf{A}(t)$ and $\mathbf{B}(t)$ are T or τ -periodic $d \times d$ matrices and \mathbf{B}_0 is a T or τ -periodic $d \times 1$ column vector. Under the above assumptions, such matrices and vectors are piecewise C^1 .

This is a system of linear, periodic delay differential equations which can be efficiently solved by the Chebyshev collocation method, as described in the next section.

The total vibration $\mathbf{q}(t)$ is generally interpreted as the sum of “static” forced vibrations due to $\mathbf{B}_0(t)$ and “dynamic” regenerative vibrations arising from the difference $(\mathbf{q}(t) - \mathbf{q}(t - \tau))$.

Under the hypothesis of constant speed machining, these terms can be studied separately by applying the superposition principle. Since the forced term is always stable, the whole stability will depend on the regenerative term, which is only influenced by $\mathbf{A}(t)$ and $\mathbf{B}(t)$. Accordingly, the stability analysis will be performed on system (74) depurated from the $\mathbf{B}_0(t)$ input [8].

6 Stability analysis

For a given combination of spindle speed and depth of cut, system stability was assessed by considering the general stability criteria of delay differential equations theory [43].

Basically, the discretization method adopted for stability evaluation approximates the infinite-dimensional monodromy operator \mathbf{U}_g representing the delay differential equations system (74) (depurated from the periodic forced excitation $\mathbf{B}_0(t)$) with a finite-dimensional transition matrix $\hat{\mathbf{U}}_g$. The stability of the system depends on the largest matrix eigenvalue, according to the following stability criterion

$$\max \left\{ |\lambda_i| : \lambda_i \in \sigma(\hat{\mathbf{U}}_g) \right\} \cong \rho < 1 \tag{75}$$

where ρ is the spectral radius of the original monodromy operator and λ_i are the eigenvalues of $\hat{\mathbf{U}}_g$.

The monodromy matrix $\hat{\mathbf{U}}_g$ is obtained from a discretization algorithm based on the Chebyshev collocation method [43–45].

The monodromy matrix size (number of columns = number of rows) is

$$D(\hat{\mathbf{U}}_g) = 2K(N + 1) + d - 2 \tag{76}$$

where d is the dimension of the state space vector $\mathbf{q}(t)$, K is the number of subintervals composing the fundamental

interval $[0, \tau]$ where the matrixes $\mathbf{A}(t)$ and $\mathbf{B}(t)$ are of class C^1 , and $N + 1$ is the number of Chebyshev collocation points for each subinterval [8]. When the number of collocation points becomes sufficiently high, the spectral radius estimate converges to the theoretical value, as shown in [8]. The algorithm was developed in the MathWorks MATLAB environment, and it was adapted and improved from the ddec MATLAB suite which was originally available on-line at (<http://www.cs.uaf.edu/>). Further technical details can be found in the above references.

7 Experimental validation

Experimental validation of the new dynamic milling model consisted of three different phases, which will be illustrated in the following sections:

1. identification of machining system dynamics through impact testing;
2. estimation of cutting force coefficients by performing dedicated cutting test;
3. determination of experimental stability lobes by performing chatter tests and comparison with model predictions.

All the experimental tests were carried out at the Laboratory for Advanced Mechatronics—LAMA FVG—located in Udine, Italy, by using a three-axes CNC milling machine Haas VF2-TR. The machine is equipped with a vertical spindle unit with nominal power $P_{el} = 22$ kW and maximum achievable spindle speed $n = 15,000$ rpm.

Several sensors were installed into the machine tool for modal analysis, cutting force measurement and chatter detection, as will be described in the following sections.

All sensor signals were sampled at 20 kHz by a National Instruments Data Acquisition device (cDAQ-9178 with NI9215 modules) and stored on a PC for further analysis, which was carried out in the MathWorks MATLAB environment.

Cutting tests were performed with a modular tooling system composed of a spindle adapter (Sandvik Coromant C5-390.140-40 030), a tool extender module (Sandvik Coromant C5-391.01-50 100A), cutter adapter (C5-391.05C-22 025M) and a milling cutter (R300-050Q22-08H) with nominal diameter $D = 50$ mm. The cutter had eight equally spaced teeth ($Z_t = 8$) consisting of round inserts (Sandvik Coromant R300-0828E-PM1030) with $r_\epsilon = 4$ mm and axial rake angle $\bar{\gamma}_a \approx 10^\circ$. In these conditions, the total tool overhang, from cutter tip to the spindle nose was about $L = 215$ mm. All the cutting tests were carried out with this tooling system setup.

In all cases, the workpiece material was Ck45 carbon steel, with about 198HB.

8 Identification of machining system dynamics

In the first phase, modal analysis was carried out on the tooling system described in the previous subsection, by means of pulse testing technique [46]. The machine dynamics were excited by means of a instrumented hammer and the vibrations were measured through accelerometers and non-contact inductive displacement sensors.

Specifically, an eddy current sensor (Micro-Epsilon type ES1 with sensitivity $\approx 10\text{mV}/\mu\text{m}$) together with a triaxial piezoelectric accelerometer Kistler 8763B100AB (sensitivity $\approx 50\text{mV}/\text{g}$) were applied for measuring cutter vibrations along all directions XYZ .

Impulsive forces were applied by means of an instrumented impact hammer type Dytran 5800B4 (sensitivity 2.41 mV/N), both in the radial and axial directions, as shown in Fig. 5a, b. By so doing, it was possible to apply both forces (F_x, F_y) and momenta (M_x, M_y) to the cutter, in order to completely identify tooling system dynamics. Radial vibrations were measured for estimating the transversal displacements u_x and u_y .

Similarly, axial vibrations of cutter periphery were measured for estimating the rotational degrees of freedom ϑ_x and ϑ_y , as can be observed in Fig. 5b, c. Pulse tests were repeated by changing sensors' locations, in order to get reliable estimates of tooling system static compliance along all directions.

Some tests were repeated after a 90° rotation of the whole tooling system (tool and spindle shaft) in order to assess the symmetry of the main spindle system.

The results are summarized in Fig. 6. It was observed that all transfer functions are independent from main spindle orientation, with good approximation.

The dynamic compliance measured at tool tip cannot be adequately represented by a single harmonic oscillator for each transversal direction, because the relatively stiff tooling system is dynamically coupled to spindle and machine dynamics as studied in [47] and [48].

Therefore, direct transfer functions $W_{u_x F_x}$ and $W_{u_y F_y}$ are characterized by several mechanical resonances, which were determined by applying a novel identification technique inspired by Wavelets theory, which is illustrated in [49]. The final modal parameters are listed in Table 1.

As evidenced in Fig. 6, there is a good correlation between experimental measurements and interpolating mathematical models. However, the most interesting result of this phase are the “secondary” transfer functions W_{u_M} , W_{ϑ_F} , and W_{ϑ_M} which relate the general degrees of freedom of the cutter tip to the general input forces acting on it, as outlined in Sections 3.1 and 3.2. In the medium frequency range where the dominant resonances are located, the measured transfer functions are almost proportional to the corresponding direct transfer functions, as predicted by Eqs. 17, 18, and 19.

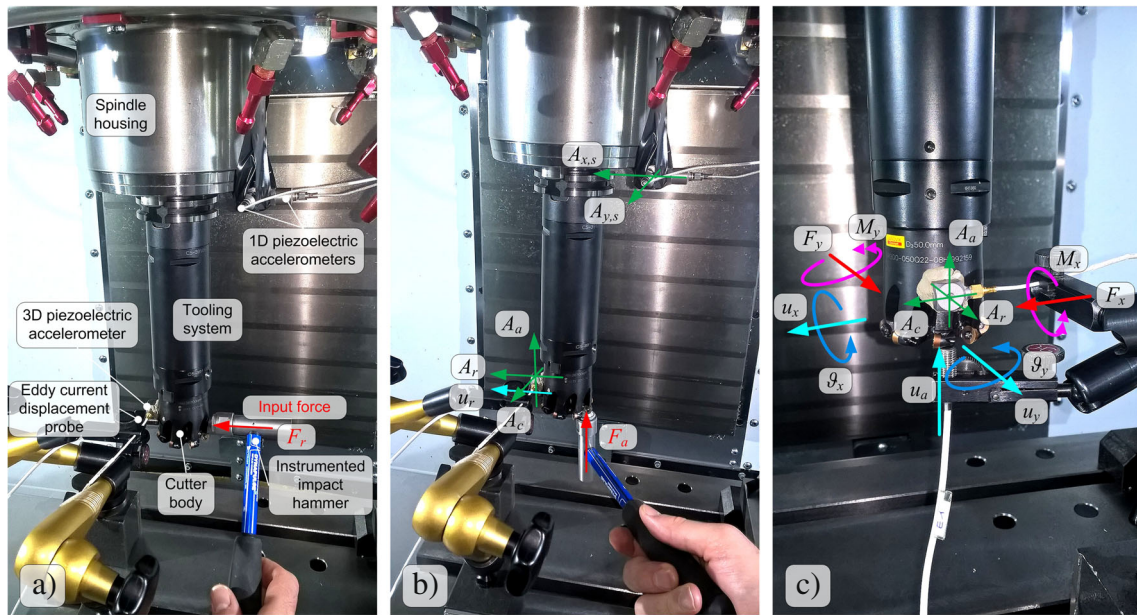


Fig. 5 Experimental modal analysis on the considered tooling system. **a** Example of experimental setup for estimating W_{uxFx} and $W_{\theta,Fx}$ by applying impulsive forces along the radial X direction. **b** Here, W_{uxMy}

is measured by applying axial forces. **c** Experimental setup for measuring W_{uyFy} , $W_{\theta,Fy}$, W_{uyMx} by applying radial and axial forces in the YZ plane

This correspondence is satisfactory along the X direction, though there are little systematic errors between model and measurements. The correlation between model and measurements is less accurate but still sufficient along the Y direction, also because it was difficult to excite regular

tooling system vibrations by applying a pure axial force (whence the low signal to noise ratio affecting W_{uyMx}).

Model inaccuracies affecting secondary transfer functions can be explained by recalling that the spindle nose was considered as a perfectly rigid constraint by the simplified

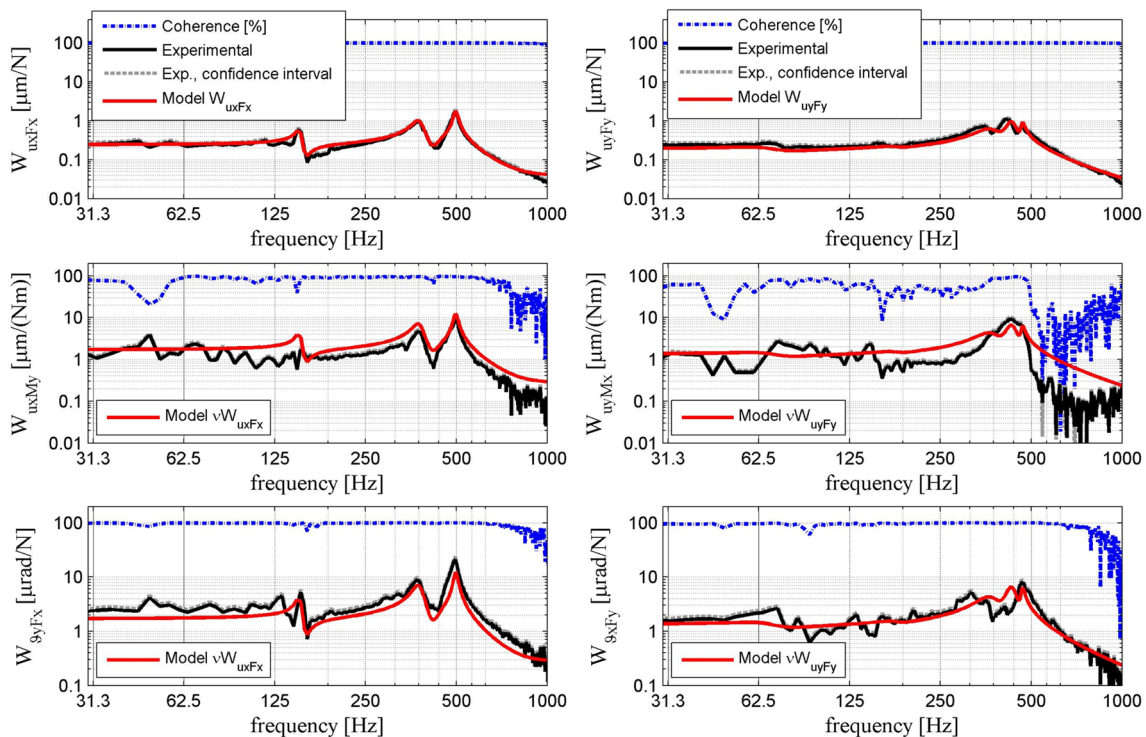


Fig. 6 Empirical transfer function estimates and comparison with the proposed model

Table 1 Estimated modal parameters of the tooling system under examination

Dir.	Mode	1	2	3	4	5
X	G_k ($\mu\text{m/N}$)	0.020	0.076	0.035	0.054	0.060
	f_k (Hz)	151.3	376.8	476.9	496.5	2000
	ξ_k []	0.0208	0.0426	0.0822	0.0173	1
	G_k ($\mu\text{m/N}$)	0.0155	0.0051	0.0882	0.0676	0.0161
Y	f_k (Hz)	69.4	177.9	370.4	428.7	466
	ξ_k []	0.1794	0.0961	0.0970	0.0420	0.0136

reference model based on Euler-Bernoulli beam theory. The proposed model does not take into account machine tool structure and spindle dynamics, as well as the effective dynamic coupling between tooling system and spindle, which was rather strong in this case study.

Eventually, $W_{\partial_x M_x}$ and $W_{\partial_y M_y}$ were disturbed by a bad signal-to-noise ratio since they were very small, as expected. For this reason, they were not even shown in Fig. 6.

However, the proposed model is capable to provide a simple and compact representation of tooling system dynamics which could be sufficient for chatter prediction purposes, as will be shown in the last section.

9 Cutting force model identification

In order to identify and validate the adopted cutting force model, specific cutting tests were carried out on a Ck45 carbon steel workpiece by using the tooling system described in Section 7. A sample workpiece was clamped on a special plate dynamometer—see Fig. 7—which was designed and validated by the author in a previous research work [52]. By using this device, instantaneous and average cutting forces were measured with great accuracy. However, for the sake of simplicity, only average cutting forces were considered for cutting force model coefficients identification.

Different cutting conditions were measured, according to the design of experiments described in Table 2. Milling operations were performed by assuming a width of cut $a_L = 19.6$ mm and lateral position $a_{L1} = 9.8$ mm, i.e., cutter barycentre was aligned with workpiece axis of symmetry.

Two complete factorial designs of experiments were executed.

The first was performed for evaluating the effect of cutting speed on average cutting forces. It consisted in the following factor levels' combinations: $3a_p \times 1f_z \times 2v_c$. In accordance with well-known classical results [53], experimental tests confirmed that cutting speed can be neglected when trying to explain the variability of average cutting forces, at least when machining simple carbon steels in a reasonable range of cutting speeds.

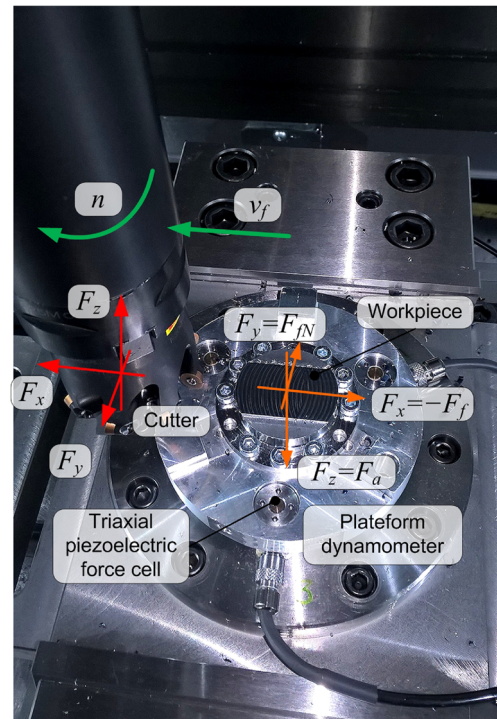


Fig. 7 Experimental setup for cutting force measurement by using special dynamometer designed and validated in [52]

The second design of experiments was eventually executed to estimate cutting force model coefficients. It consisted in the following factor levels' combinations: $3a_p \times 3f_z \times 1v_c$.

Average cutting forces are visible in the scatter diagram of Fig. 8.

The final regression was accomplished by considering the algebraic system

$$\bar{\mathbf{F}}_{exp} = \mathbf{X} \mathbf{k} + \varepsilon \tag{77}$$

where the known term was composed by $3N$ rows

$$\bar{\mathbf{F}}_{exp} = [\bar{F}_{x1} \dots \bar{F}_{xN} \bar{F}_{y1} \dots \bar{F}_{yN} \bar{F}_{z1} \dots \bar{F}_{zN}]_{exp}^T \tag{78}$$

while the vector of unknown S&P coefficients was

$$\mathbf{k} = [k_{cs} \ k_{cp} \ k_{ns} \ k_{np}]^T \tag{79}$$

Table 2 Design of experiments for estimation of cutting force model

Factor	Levels	Values
Depth of cut a_p (mm)	3	0.2, 0.4, 0.6
Feed per tooth f_z (mm)	1 ÷ 3	0.12, 0.18, 0.24
Spindle speed n (rpm)	1 ÷ 2	1600, 2400
(Cutting speed v_c (m/min))		(230, 350)

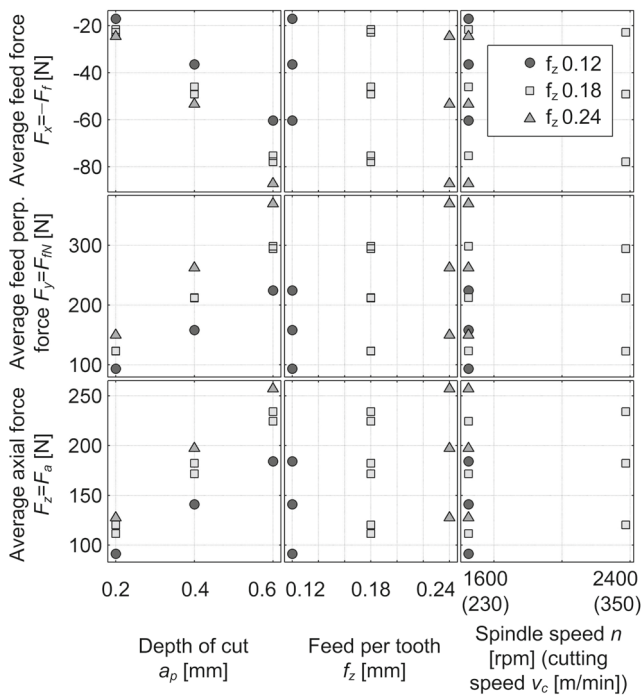


Fig. 8 Average experimental forces along the X, Y, and Z directions of the stationary reference frame

Matrix **X** is obtained by integrating Eq. 41 with respect to time (or equivalently, with respect to the reference feed motion angle φ for all experimental conditions, by taking into account tool geometry and the effective tool-workpiece engagement, see [24] for further details.

Optimal values of S&P coefficients enclosed into the vector \mathbf{k}_{opt} were determined by the classical pseudo-inverse formula and are listed in Table 3. Accordingly, the average cutting forces estimated by the model were determined as usual

$$\bar{\mathbf{F}}_{mod} = \mathbf{X} \mathbf{k}_{opt} \quad (80)$$

Eventually, the relative residues between model estimates and effective experimental values were computed (Fig. 9), i.e.,

$$E_{w,R} = \frac{\bar{F}_{wi,mod} - \bar{F}_{wi,exp}}{R_{i,exp}} [\%] \quad w = x, y, z \quad (81)$$

where the normalization was carried out by using the modulus of the resultant average force, that is

$$R_{i,exp} = \sqrt{\bar{F}_{xi,exp}^2 + \bar{F}_{yi,exp}^2 + \bar{F}_{zi,exp}^2} \quad (82)$$

Table 3 Estimated cutting force coefficients

k_{cs} (N/mm ²)	k_{cp} (N/mm)	k_{ns} (N/mm ²)	k_{np} (N/mm)
1909	33	1020	48

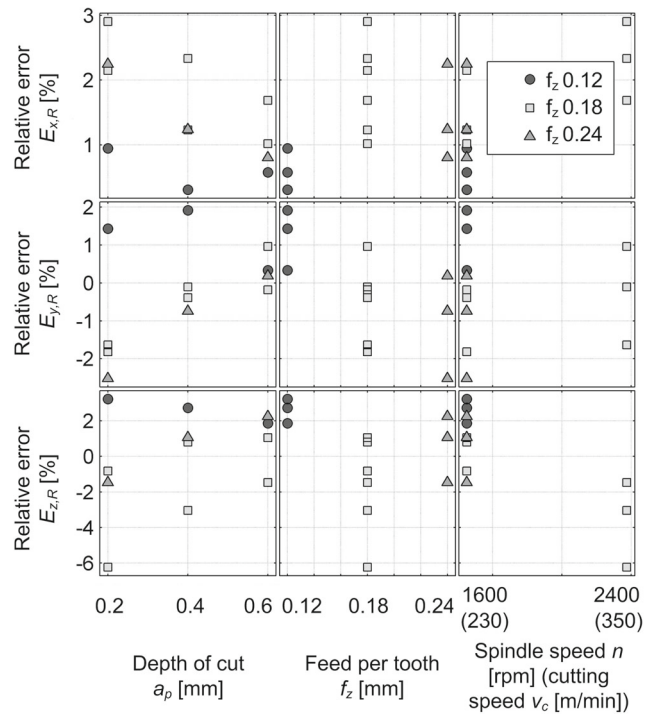


Fig. 9 Relative errors between average forces estimated by the adopted model and the effective experimental values, along the X, Y, and Z directions of the stationary reference frame

Some indexes for evaluating cutting force model adequacy are listed in Table 4. In conclusion, the obtained model is able to explain most of the variability of the observed cutting force trends by using only four coefficients, confirming the effectiveness of modern S&P models inspired by oblique cutting theory, in comparison to other pure mechanistic/mathematical approaches based on a greater number of coefficients [25, 50].

Eventually, the regenerative cutting force coefficients k_c , k_r , and k_a could be calculated by applying Eq. 63, as illustrated in Fig. 10 for the case study examined in this work. The new coefficients can be compared to the classical model, which is simply

$$\begin{cases} k_{c,classic}(a_p) = k_{cs} a_p \\ k_{r,classic}(a_p) = k_{ns} a_p \\ k_{a,classic}(a_p) = 0 \end{cases} \quad (83)$$

Table 4 Cutting force model adequacy

Index	X	Y	Z
Squared linear corr. coeff. R^2 []	0.994	0.999	0.988
Standard dev. of rel. error σ (%)	0.8	1.3	2.7
Systematic relative error μ (%)	1.5	-0.2	-0.0

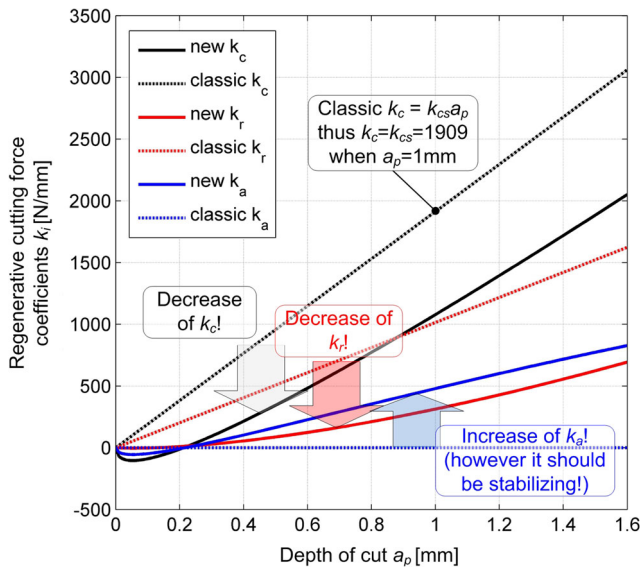


Fig. 10 Behavior of regenerative cutting force coefficients k_c , k_r , and k_a and comparison with classical model ($k_{cs} = 1909$ MPa, $k_{ns} = 1020$ Mpa, $a_p < r_E = 4$ mm, as in the real case study discussed in the following sections)

Of course, the new model of regenerative cutting force coefficients reduces to the classical relations (83) when considering straight cutting edges with $\chi \equiv 90^\circ$ and $\gamma_a \equiv 0^\circ$.

Nevertheless, for generic cutting edge geometries, the difference between the new and the classical model can be very large, thus having a great impact on chatter onset prediction.

10 Final validation by means of chatter tests

In order to validate the new model and to show its predictive capabilities, a specific experimental campaign was conceived and carried out.

Table 5 Design of experiments for chatter tests

Factor	Lev.	Values
Depth of cut a_p (mm)	7	0.4, 0.6, 0.7, 0.75, 0.8, 0.85, 0.9
Spindle speed n (rpm)	16	increments of 80 from 1000 to 2200
(Cutting speed v_c (m/min))		(increments of 12 from 150 to 330)

Centered milling operations with $a_L = 34$ mm, $a_L/D \approx 75\%$, and $a_{L1} = 17$ mm were executed in order to allow stability borders identification in a reasonable range of depths of cut, in the perspective of avoiding any damage to the machine tool. Feed per tooth was set to 0.18 mm for all the cutting tests. Experimental setup during chatter tests is illustrated in Fig. 11.

A grid of cutting parameter combinations was tested, as summarized in Table 5.

The depth of cut was increased by discrete increments of $0.2 \div 0.05$ mm until severe chatter occurred. The test was stopped at a maximum depth of cut of 0.9 mm if no chatter was observed.

The stability of the system was assessed both from visual inspection and by calculating quantitative chatter indicators [54] obtained from the accelerometers installed on spindle housing, as illustrated by the examples reported in Figs. 11 and in 12.

It is worth noting that chatter vibrations arising in the considered case study were particularly explosive and violent, and they tended to propagate to the machine tool structure instead of being merely restricted to the tooling system. This behavior can be explained by

- the strong dynamic coupling between tooling system and spindle dynamics, resulting in the mechanical resonance at about 300 Hz;

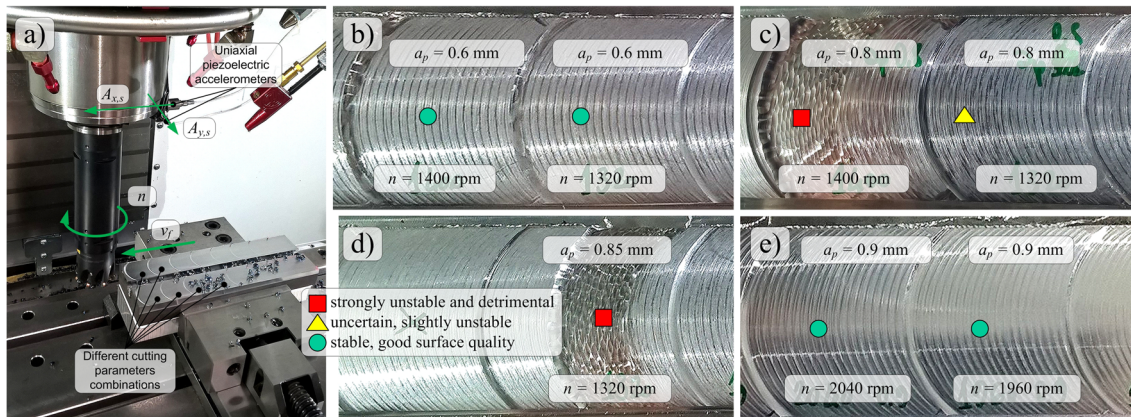


Fig. 11 Experimental setup for chatter tests and examples of machined surfaces under different cutting parameters combinations

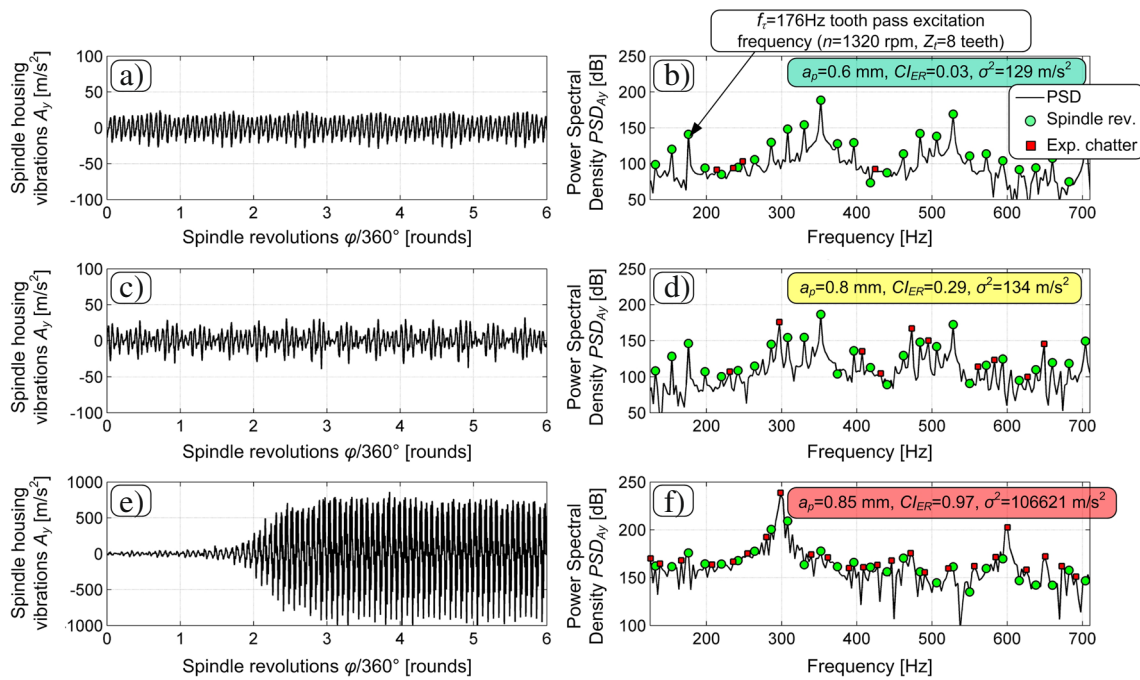


Fig. 12 Example of signal characteristics in time and frequency domains when considering cutting tests performed at $n = 1320$ rpm

- the high inertial forces exchanged between tooling system and spindle, due to the large tooling system mass, which was significantly greater in comparison with the slender tooling systems with small cutter diameter which are typically investigated in literature.

Moreover, chatter phenomena were somehow amplified by the strong axial vibrations of each cutting tooth—coupled to the large transverse vibrations of cutter barycentre, as explained in Section 3—which may have dramatically altered the tooth-workpiece engagement conditions, as evidenced by the impressive chatter marks visible in Fig. 11.

For all these reasons, the relatively small threshold of $a_p \leq 0.9$ mm was adopted in order to avoid damaging the machine tool elements, such as the spindle bearings.

I would like to warn other researchers who want to continue the research in this field to be particularly careful when performing chatter tests in similar conditions.

The stability analysis was carried out by the Chebyshev Collocation Method recalled in Section 6.

In the considered case study, there are five harmonic oscillators along the X direction and five harmonic oscillators along the Y direction, for a total of ten independent harmonic oscillators included in the tooling system transfer functions, Table 1. Thus, the size of the square matrix \mathbf{A} is $d = 10 \cdot 2 = 20$.

Apparently, the new approach seems to require a greater matrix size d since it introduces new degrees of freedom (ϑ_x and ϑ_y) in addition to the classical displacements u_x and u_y . Nevertheless, it is important to recall that rotational and

translational degrees of freedom are different viewpoints of the same eigenmodes. In the current case, they are even assumed proportional to each other thanks to the reasonable assumption (10). Accordingly, the classical model and the new model are based on the same number of independent harmonic oscillators and hence on the same matrix size d . Therefore, the new model significantly improves and refines the classical model by keeping the same computational complexity.

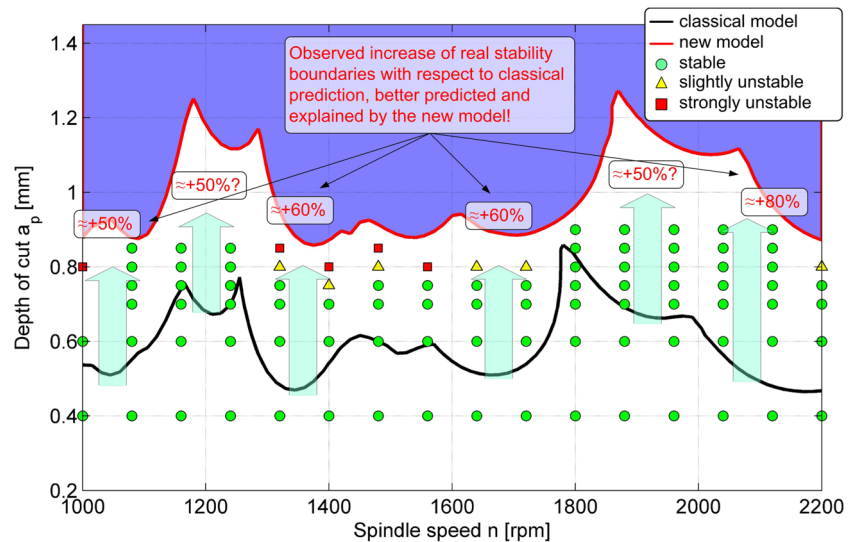
In the case study under interest, there is at least one kink within the fundamental time interval of length τ , provided that the entrance is taken as starting point ($\varphi = \varphi_{in}$). Thus, $K = 2$ in Eq. 76. Some preliminary numerical investigations were performed in order to determine an adequate matrix size $D(\hat{\mathbf{U}}_g)$ for assuring a good accuracy of the estimated spectral radius. It was assessed that a good accuracy

$$\left| \frac{\hat{\rho} - \rho_{th}}{\rho_{th}} \right| < 0.001 \% \tag{84}$$

could be achieved in this case by adopting $D(\hat{\mathbf{U}}_g) = 162$, which corresponded to a number of Chebyshev collocation points equal to $N + 1 = 36$. The predicted stability lobes were determined by calculating a grid of about 80 spindle speed levels \times 40 depth of cut levels.

The obtained results (Fig. 13) evidenced that the classical model does significantly underestimate the effective stability boundaries (more than 50 % of estimate error). On the contrary, the new approach is much closer to the observed

Fig. 13 Comparison between experimental and predicted stability lobes



stability lobes, although a slight overestimation likely due to the uncertainties affecting the identified model coefficients and to other reasonable error sources [14].

The increase of the stability boundaries predicted by the new model can now be physically interpreted through the reduction of the regenerative chip thickness (50) and the stabilizing effect of the axial forces (13).

Moreover, the innovation provided by the new analytical formulation of regenerative cutting force coefficients (52 and 63) has managed to significantly reduce the computation time associated to spectral radius estimate.

The computation is performed in two phases. In the first phase, all the information regarding the cutting process for a given combination of cutting parameters is assigned to a Matlab object, which is a structure including the state space matrixes **A** and **B**, the considered cutting parameters, et cetera. Afterwards, the monodromy matrix is derived and spectral radius estimate is calculated.

Let us now focus on this latter phase, whose computation time was deeply discussed in [8]. In accordance to that work, the computation time had to be about 0.045 s when monodromy matrix was 162×162 , as in the current case (of course, when using a similar PC).

When performing this calculation according to the incremental/differential approach proposed in [24] for regenerative cutting force coefficient determination, a much longer computation time of about 0.63 s was observed, which was also due to the larger state space matrix size ($d = 20$ instead of $d = 4$ as in [8]).

However, when exploiting the new integral formulation based on the direct analytical expressions (63), the computation time drops to about 0.33 s, with a relative reduction of about -47% .

Thus, a significant gain of computational speed was achieved through the proposed improvements.

11 Conclusions

According to the considerations and results presented in this work, we may draw the following conclusions.

In a very recent work [24], a new model of milling dynamics including the effect of additional rotational degrees of freedom and bending momenta associated to axial forces was introduced and validated on a case study where such effects were significant but still moderate.

However, one key result of that work was a new formula for regenerative chip thickness estimation which incorporated the effect of cutting edge curvature (local χ) and the coupling between the axial and radial vibrations of each tooth (depending on the aspect ratio D/L). Moreover, regenerative forces were correctly oriented in three-dimensional space, again by considering the local curvature of the cutting edge. By summing up all the contributions, the final regenerative force coefficients in the tangential (k_c), radial (k_r), and axial (k_a) directions could be determined, according to an iterated incremental procedure which should be repeated for every cutting parameters combination (n, a_p).

Here a new mathematical formulation was proposed—which is mainly valid for inserted cutters—based on the analytical solution of the integrals defining the regenerative cutting force coefficients, which can be preliminarily determined before launching the calculation of the stability lobe diagrams. For standard cutting inserts, these formulas are basic functions of cutting edge geometry (χ_1 and r_ε) and of the shearing force coefficients k_{cs} and k_{ns} .

In addition, a new impressive experimental validation of the new model of milling dynamics was presented in this work, by using a face milling cutter with round inserts ($D = 50$ mm, $Z_t = 8$ teeth, $r_\varepsilon = 4$ mm) tested on carbon steel in centered milling configuration, with $a_L/D \approx 75\%$.

The following conclusions were obtained from the new experimental benchmark:

- Secondary transfer functions $W_{\vartheta F}$ and W_{uM} are almost proportional to the corresponding direct transfer functions W_{uF} by means of the proportionality constants proposed in section 3; however, some discrepancies were observed, which were likely due to the unmodelled dynamic coupling between tooling system and spindle; nevertheless, even in this case the new model is capable of providing a better but still simple and compact representation of tooling system dynamics.
- For generic cutting edge geometries, the differences between the new and the classical expressions of the regenerative cutting force coefficients may be very large; therefore, the impact of new formulation on the accuracy of the predicted stability borders may be great in many practical circumstances.
- Chatter vibrations observed in these conditions may be really violent and detrimental for the whole machine tool, thus remarking the importance of absolutely avoiding the onset of regenerative chatter in other similar applications.
- The classical model does significantly underestimate the effective stability boundaries (more than 50 % of estimate error). On the contrary, the new approach is much closer to the observed stability lobes.
- The increase of the stability boundaries predicted by the new model can now be physically interpreted through the reduction of the regenerative chip thickness (Eq. 46) and the stabilizing effect of the axial forces (Eq. 13).
- A significant reduction of about –45 % of computation time was observed when performing the stability analysis, thus demonstrating the gain in computational speed achieved through the algorithmic improvements implemented here.

In the future, it will be of strong interest to exploit the predictive power of the new model for optimizing real industrial applications.

Acknowledgments The Laboratory for Advanced Mechatronics - LAMA FVG—is gratefully acknowledged for technical support. LAMA FVG is an international research center for product and process innovation where the three Universities of Friuli Venezia Giulia Region (Italy) synergically cooperate for promoting R&D activities. Sandvik Coromant Italy is also gratefully acknowledged for technical support. Special thanks are dedicated to Mr. Lucio Simonato and Mr. Stefano Pagnutti, who gave a precious contribution for setting up the experimental configuration.

References

1. Stepan G (1998) Delay-differential equation models for machine tool chatter. In: Moon FC (ed) Nonlinear dynamics of material processing and manufacturing. Wiley, New York, pp 165–169
2. Altintas Y, Weck M (2004) Chatter stability of metal cutting and grinding. *Ann CIRP* 53(2):619–642
3. Sortino M, Totis G, Prospero F (2013) Modeling the dynamic properties of conventional and high-damping boring bars. *Mech Sys Sig Proc* 34:340–352
4. Budak E (2003) An analytical design method for milling cutters with nonconstant pitch to increase stability. Part 2: application. *J Manuf Sci Eng Trans ASME* 125:35–38
5. Weck M, Brecher C (2006) *Werkzeugmaschinen 5: Messtechnische Untersuchung und Beurteilung, dynamische Stabilität*. Springer
6. Mei D, Konga T, Shihb AJ, Chen Z (2009) Magnetorheological fluid-controlled boring bar for chatter suppression. *J Mater Process Technol* 209:1861–1870
7. Segalman DJ, Butcher EA (2000) Suppression of regenerative chatter via impedance modulation. *J Vib Control* 6(2):243–256
8. Totis G, Albertelli P, Sortino M, Monno M (2014) Efficient evaluation of process stability in milling with Spindle Speed Variation by using the Chebyshev Collocation Method. *J Sound Vib* 333:646–668
9. Dohner JL, Lauffer JP, Hinnerichs TD, Shankar N, Regelbrugge M, Kwan CM, Xu R, Winterb B (2004) Mitigation of chatter instabilities by active structural control. *J Sound Vib* 269:197–211
10. Brecher C, Manoharan D, Ladra U, Köpken HG (2010) Chatter suppression with an active workpiece holder. *Prod Eng Res Devel* 4:239–245
11. van Dijk NJM, Doppenberg EJJ, Faassen RPH, van de Wouw N, Oosterling JAJ, Nijmeijer H (2010) Automatic in-process chatter avoidance in the high speed milling process. *ASME J Dyn Syst Meas Control* 132:1–14
12. Gradisek J, Kalveram M, Insperger T, Weinert K, Stepan G, Govekar E, Grabec I (2005) On stability prediction for milling. *Int J Mach Tools Manuf* 45:768–781
13. Altintas Y, Stepan G, Merdol D, Dombovari Z (2008) Chatter stability of milling in frequency and discrete time domain. *CIRP J Manuf Sci Technol*. 1:35–44
14. Totis G (2009) RCPM—a new method for robust chatter prediction in milling. *Int J Mach Tools Manuf* 49:273–284
15. Tobias A (1965) *Machine tool vibration*. Blackie and Sons Ltd
16. Sellmeier V, Denkena B (2012) High speed process damping in milling. *CIRP J Manuf Sci and Technol* 5:8–19
17. Ahmadi K, Ismail F (2012) Stability lobes in milling including process damping and utilizing multi-frequency and semi-discretization methods. *Int J Mach Tools Manuf* 54-55:46–54
18. Grabec I (1988) Chaotic dynamics of the cutting process. *Int J Mach Tools Manuf* 28:19–32
19. Warminski J, Litak G, Cartmell MP, Khanin R, Wiercigroch M (2003) Approximate analytical solutions for primary chatter in the non-linear metal cutting model. *J Sound Vib* 259(4):917–933
20. Davies MA, Burns TJ, Evans CJ (1997) On the dynamics of chip formation in machining hard materials. *Ann CIRP* 46:25–30
21. Sisson TR, Kegg RL (1969) An explanation of low speed chatter effects. *J Eng Ind Trans ASME*:951–958
22. Tlustý J (1978) Analysis of the state research in cutting dynamics. *Ann CIRP* 2:583–589
23. Altintas Y, Budak E (1995) Analytical prediction of stability lobes in milling. *Ann CIRP* 44:357–362
24. Totis G, Albertelli P, Torta M, Sortino M, Monno M (2017) Upgraded stability analysis of milling operations by means of advanced modeling of tooling system bending. *Int J Mach Tools Manuf* 113C:19–34. doi:10.1016/j.ijmactools.2016.11.005
25. Altintas Y (2000) *Manufacturing automation: metal cutting mechanics, machine tool vibrations and CNC design*. Cambridge University Press
26. Campa FJ, Lopez de Lacalle LN, Celaya A (2011) Chatter avoidance in the milling of thin floors with bull-nose endmills: model and stability diagrams. *Int J Mach Tools Manuf* 51:43–53

27. Budak E, Tunc LT, Alan S, Ozguven HN (2012) Prediction of workpiece dynamics and its effects on chatter stability in milling. *CIRP Ann - Manuf Technol* 61:339–342
28. Insperger T, Stepan G, Bayly PV, Mann BP (2003) Multiple chatter frequencies in milling processes. *J Sound Vib* 262:333–345
29. Mann BP, Insperger T, Bayly PV, Stepan G (2003) Stability of up-milling and down-milling, part 2: experimental verification. *Int J Mach Tools Manuf* 43:35–40
30. Govekar E, Gradisek J, Kalveram M, Insperger T, Weinert K, Stepan G, Grabec I (2005) On stability and dynamics of milling at small radial immersion. *CIRP Ann* 54(1):357–362
31. Catania G, Mancinelli N (2011) Theoretical experimental modeling of milling machines for the prediction of chatter vibration. *Int J Mach Tools Manuf* 51:339–348
32. Sellmeier V, Denkena B (2011) Stable islands in the stability chart of milling processes due to unequal tooth pitch. *Int J Mach Tools Manuf* 51:152–164
33. Wan M, Ma YC, Zhang WH, Yang Y (2015) Study on the construction mechanism of stability lobes in milling process with multiple modes. *Int J Adv Manuf Technol* 79:589–603
34. Kilic ZM, Altintas Y (2016) Generalized mechanics and dynamics of metal cutting operations for unified simulations. *Int J Mach Tools Manuf* 104:1–13
35. Zou GP, Yellowley I, Seethaler RJ (2009) A new approach to the modeling of oblique cutting processes. *Int J Mach Tools Manuf* 49:701–707
36. Wan M, Pan WJ, Zhang WH, Ma YC, Yang Y (2014) A unified instantaneous cutting force model for flat end mills with variable geometries. *J Mater Process Technol* 214:641–650
37. Wan M, Ma YC, Feng J, Zhang WH (2016) Study of static and dynamic ploughing mechanisms by establishing generalized model with static milling forces. *Int J Mech Sci* 114:120–131
38. Dombovari Z, Altintas Y, Stepan G (2010) The effect of serration on mechanics and stability of milling cutters. *Int J Mach Tools Manuf* 50:511–520
39. Yusoff AR, Sims ND (2011) Optimisation of variable helix tool geometry for regenerative chatter mitigation. *Int J Mach Tools Manuf* 51:133–141
40. Stepan G, Munoa J, Insperger T, Surico M, Bachrathy D, Dombovari Z (2014) Cylindrical milling tools: Comparative real case study for process stability. *CIRP Ann - Manuf Technol* 63:385–388
41. Campomanes ML, Altintas Y (2003) An improved time domain simulation for dynamic milling at small radial immersions. *Manuf Eng Sci Trans ASME* 125:29–38
42. Moradi H, Movahhedy MR, Vossoughi G (2012) Dynamics of regenerative chatter and internal resonance in milling process with structural and cutting force nonlinearities. *J Sound Vib* 331:3844–3865
43. Bueler E (2004) Chebyshev Collocation for Linear, Periodic, Ordinary and Delay Differential Equations: a Posteriori Estimates. Cornell University Library. arXiv:0409464
44. Bueler E, Butcher E (2003) Stability of periodic linear delay-differential equations and the Chebyshev approximation of fundamental solutions. UAF Department of Mathematical Sciences Technical Report, pp 2002–2003
45. Trefethen LN (2000) Spectral methods in MATLAB. SIAM Press, Philadelphia
46. Ewins DJ (2009) Modal testing: theory, practice and application, 2nd. Wiley. ISBN: 978-0-86380-218-8
47. Albertelli P, Cau N, Bianchi G, Monno M (2012) The effect of dynamic interaction between machine tool subsystems on cutting process stability. *Int J Adv Manuf Technol* 58(9-12):923–932
48. Kolar P, Sulitka M, Janota M (2011) Simulation of dynamic properties of a spindle and tool system coupled with a machine tool frame. *Int J Adv Manuf Technol* 54(1):11–20
49. Totis G, Sortino M, Belfio S (2016) Wavelet-like analysis in the frequency-damping domain for modal parameters identification. In: Proceedings of the 26th DAAAM international symposium on intelligent manufacturing and automation. Wien, pp 580–588. doi:10.2507/26th.daaam.proceedings.079
50. Kao YC, Nguyen NT, Chen MS, Huang SC (2015) A combination method of the theory and experiment in determination of cutting force coefficients in ball-end mill processes. *J Comp Des Eng* 2:233–247
51. Totis G, Sortino M (2013) Robust analysis of stability in internal turning. In: 24th DAAAM international symposium on intelligent manufacturing and automation, vol 69. Procedia Engineering, pp 1306–1315
52. Totis G, Adams O, Sortino M, Veselovac D, Klocke F (2014) Development of an innovative plate dynamometer for advanced milling and drilling applications. *Meas* 49:164–181
53. Micheletti GF (1977) Tecnologia meccanica I - Il Taglio dei Metalli. UTET, Torino
54. Kuljanic E, Sortino M, Totis G (2008) Multisensor approaches for chatter detection in milling. *J Sound Vib* 312:672–693